Journal of Cluster Science (2018) 29:1003–1015
https://doi.org/10.1007/s10876-018-1411-5

ORIGINAL PAPER

Synthesis of Metallic Silver Nanoparticles by Fluconazole Drug and Gamma Rays to Inhibit the Growth of Multidrug-Resistant Microbes

Ahmed I. El-Batal[1] · Farag M. Mosallam[1] · Gharieb S. El-Sayyad[1]

Received: 14 May 2018 / Published online: 13 June 2018

Abstract
Here we tailored a methodology, including green synthesis of silver nanoparticles (AgNPs) in aqueous solution using Fluconazole (Fluc.), a broad-spectrum antifungal agent under the influence of gamma rays. AgNPs were characterized by UV–Vis., FTIR, XRD, DLS, and TEM image. Antimicrobial activities of AgNPs, Fluc., and Ag^{+} were investigated against multidrug-resistant (MDR) bacteria and unicellular fungi. From our results, AgNPs production was found to be dependent on the concentration of Ag^{+}, Fluc. and gamma doses. DLS with TEM image explained the size and shape of AgNPs and were found to be spherical with diameter of 11.65 nm. FTIR analysis indicates that, the hydroxyl, nitrogen and fluoride moiety in Fluc. were responsible for the reduction and binding process. AgNPs possesses antimicrobial activity against all tested microbes more than Ag^{+}. It produced high efficacy against *Acinetobacter baumannii* (20.0 mm ZOI). AgNPs are synergistically active towards *Candida albicans* (17.0 mm ZOI). Investigated action mechanisms for AgNPs activity had been discussed. Thereby, owing to its unique features as cost-effective with continued-term stabilization, it can discover potential targets in biomedical applications and infectious diseases control.

Keywords Fluconazole · Silver nanoparticles · Gamma irradiation · Synergism · Antibacterial activity

Introduction

In current times, the development of effective green methods for the synthesis of metal nanoparticles has displayed a significant focus of studies [1–3]. Nanoparticles production and utilization are getting great interest in biomedicine, biological control, industry, and agriculture [3, 4]. The smaller size of nanoparticles, large surface area, and reactivity was afforded them the special capacity for therapeutic design, pharmacology, parasitology and entomology in various dosage patterns [5].

Nanoparticles could be obtained from many roots of gas, liquid or solid forms. They can be manufactured utilizing diverse artificial methods like biological, physical, and chemical synthesis [5–9]. Gamma irradiation has been demonstrated to be an easy way for nanoparticles synthesis which needs an aqueous mode, room temperature, and pressure [10–13].

AgNPs have been broadly utilized for various purposes, such as room sprays, pharmaceutical devices, refrigerators, washing tools and textiles [1, 2, 7, 14–16]. The antimicrobial actions of AgNPs had been investigated, although the mechanism required and the cytotoxic consequences toward human cells become not been examined [7, 17].

Fluconazole has chemical name a bis-triazodifluorophenyl-2-propanol, and antifungal composite including both in vivo and in vitro action upon *Candida albicans* [18, 19].

Electronic supplementary material The online version of this article (https://doi.org/10.1007/s10876-018-1411-5) contains supplementary material, which is available to authorized users.

✉ Gharieb S. El-Sayyad
Gharieb.Elsayaad@eaea.org.eg; adham_adham699@yahoo.com

Ahmed I. El-Batal
Ahmed.Elbatal@eaea.org.eg; aelbatal2000@gmail.com

Farag M. Mosallam
Farag.abomosalam@eaea.org.eg; farag3m2012@gmail.com

[1] Biotechnology Division, Drug Radiation Research Department, Drug Microbiology Laboratory, National Center for Radiation Research and Technology (NCRRT), Atomic Energy Authority, Cairo, Egypt

Association of nanoparticle surfaces with drug particles is engaging for many biomedical treatments [20, 21]. With the appearance of exceptional techniques to integrate different nano-materials with unique control up the shape and size, they were gaining potential usage in biology and medicine [7, 22–24].

The methods of conjugating drug units (particularly antibiotics) with metal nanoparticles remain a complicated, also the chemical synthesis including various levels such as the production of metal nanoparticles, their surface adjustment, and certainly the capping of drug particles was interesting [25].

The emergency of Fluc. and another antimicrobial standard such as Amphotericin B and Nystatin resistance in certain fungi has increased investigation on different antifungal factors [1, 2, 12, 26]. So, nanotechnology presents the best principles to tackle this disadvantage, different particles in nanometer scale can be practiced as an antifungal tool as well as the vehicle for distribution of active elements to the targeted position externally changing the action of the current material [1, 27].

In this regard, we have decided for the first time, Fluc. (the antifungal drug), as a prototype model to illustrate an uncomplicated one-pot green synthesis and assembly of AgNPs, as well as their capping outwardly the treatment of any undesired chemicals following the influence of gamma irradiation. After that, the examination of the antimicrobial synergistic impact of AgNPs towards remarkable decided multidrug-resistant bacteria, standard bacterial isolates, and unicellular pathogenic fungi had been investigated. The investigated action mechanism of the synthesized AgNPs was illustrated.

Materials and Methods

Chemicals and Reagents

Media constituents were obtained from (Oxoid) and (Difco). Chemicals (Fluc., silver nitrate) and reagents utilized in the following examinations and biological experiments were received at analytical standard grade (Sigma-Aldrich), and appropriated without additional purification.

Radiation Source

The method of gamma irradiation was conducted out at the NCRRT, Cairo, Egypt. The irradiation source was ^{60}Co-Gamma chamber 4000-A-India. Gamma rays were delivered using ^{60}Co gamma rays at a dose rate 2.08 kGy/h at the time of the test. In this process, ^{60}Co gamma rays combine with materials in the solution essentially by photoelectric absorption and Compton scattering to generate free and hydrated induced electrons of water radiolysis.

Synthesis of AgNPs

AgNPs were synthesized through Fluc. (as a stabilizing agent) and gamma-ray (as reducing agent). Experimental factorial studies (Table S1) were comparing the impact of the concentration and radiation dose on AgNPs production. The investigated factorial study was consists of three variables in two level, concentration of (silver ions, Fluc.) and radiation dose. The main reasons for factors chosen from the recent literature that, they have the most meaningful impact on AgNPs synthesis.

Silver nitrate solution (at different Conc. shown in Table S1) was combined with Fluc. solution (at different Conc.) at ratio (1:1) v/v with (0.2%) isopropanol being a free radical collector. The mixtures were stirred at an ambient temperature (25.0 ± 2 °C) and exposed to different gamma ray. UV–visible responses (O.D.) estimated the main influences of parameters on AgNPs synthesis.

The statistical software package (Minitab 16, USA) applied for planning the test, regression, interpretation of test data and in planning the association among variables.

Characterization of AgNPs

Characterization of AgNPs was performed by UV–Visible spectrophotometer (JASCO V-560. UV–Vis. Spectrophotometer from 200–900 nm at a resolution of 1.0 nm) using the irradiated control (negative) for autozero support.

Average particle size of an incorporated AgNPs and size distribution were estimated by Dynamic Light Scattering (DLS-PSS-NICOMP 380-ZLS particles sized system St. Barbara, California, USA). 200 µL of AgNPs carried to a disposable little cuvette. Following equilibration to a temperature of 25.0 ± 2 °C for 2.0 min., five measures were implemented.

The morphology (shape of nanoparticles) and size of AgNPs were notified by using TEM image (JEOL electron microscopy JEM-100 CX). Drop coating AgNPs produced TEM examinations onto carbon-coated TEM grids after drying by incubation at 37.0 ± 2 °C in an incubator.

X-ray diffraction analysis was used to determine the crystalline shape of the synthesized AgNPs. It was adjusted with the XRD-6000 lists, including outstanding austenite quantitation, crystallinity estimation, stress examination, and crystallite size/lattice strain matters. The investigation of extended X-ray diffraction models (Shimadzu apparatus) was employed Cu-Kα target, and nickel filter (Shimadzu Scientific Instruments; SSI, Japan). Working by a Cu anode at 50.0 mA and 40.0 kV in the state of 2θ value inside 20° and 100° with a flow of 2°/min.; the intensity of the

diffracted X- rays estimated as a function of the diffracted angle 2θ.

Finally, FT-IR investigation was a helpful method that provides information regarding chemical functional groups remaining in the Fluc. drug. The measures were carried out by a JASCO FT-IR 3600 Infra-Red spectrometer by working KBr Pellet purpose. It was recorded at a resolution of 4.0 cm^{-1} in a wave number range of 400–4000 cm^{-1}.

Determination of the Antimicrobial Activity of AgNPs, Fluc., and Ag^+

AgNPs (synthesized by Fluc.; 2.0 mg/mL, and the effect of gamma irradiation; 5.0 kGy), Fluc.; 2.0 mM (the negative control) and silver ions; Ag^+; 1.5 mM (the positive control) were tested for the antimicrobial activity, applying the agar well distribution procedure [2, 12, 16, 20, 28–31].

Additionally, AgNPs, Fluc., and Ag^+ were tested upon several isolates of multidrug-resistant bacteria obtained kindly from Drug Microbiology laboratory, Drug Radiation Research department, NCRRT, Cairo, Egypt. The examined pathogens include Gram-positive bacteria (*Staphylococcus epidermidis*, *Staphylococcus aureus*; MRSA, and *Enterococcus faecalis*) and Gram-negative bacteria (*Acinetobacter baumannii*, *Enterobacter cloacae* and *Escherichia coli*).

The multidrug-resistant bacteria were examined and, recognized by Vitek® two systems (bioMarieux, Marcy-LEtoile, France) [32]. Furthermore, all remained resistant to antibiotics especially, Cefoxitin, Ampicillin, Gentamycin, Colistin, Meropenem, Cephalexin, Cefotaxime, Piperacillin-Tazobactam, Ceftazidime, Cefapirin, and Imipenem. On the other hand, AgNPs, Fluc., and Ag^+ ions were investigated for the antibacterial action upon standard strains of Gram-negative bacteria (*Klebsiella pneumoniae* ATCC 4352, *Pseudomonas aeruginosa* ATCC 27853, *Escherichia coli* ATCC 25922) and Gram-positive bacteria (*Bacillus subtilis* ATCC 6633, *Enterococcus faecalis* ATCC 29212, and *Staphylococcus aureus* ATCC 29213).

Additionally AgNPs, Fluc., and Ag^+ ions were examined for their potential as antibacterial factors against *Mycobacterium tuberculosis* RCMB 010126 obtained kindly from The Regional Center For Mycology And Biotechnology (RCMB), Faculty of science, Al-Azhar University, Cairo, Egypt.

Furthermore, an antifungal activity was tested toward unicellular fungi (*Candida albicans* ATCC 10231). The growth inhibition of all examined microbial pathogens was determined by Zone of Inhibition (ZOI) after 24 h. plates incubation [2, 13, 30].

Standard common antibiotic discs (6.0 mm diameter) like Amoxicillin/Clavulanic Acid (AMC; 20/10 µg/mL) besides, Nystatin (NS 100; 100 µg/mL) [26], were applied to estimate the impact of the synthesized AgNPs.

The minimum inhibitory concentrations (MIC) determination was investigated in Luria–Bertani (LB) broth in duplicate, performing two-fold successive dilutions of Fluc., the synthesized AgNPs, and Ag^+ [2, 31]. In these methods, a positive control well (the nutrient, and the microorganism), and negative control one (the nutrient alone) had been associated. MIC was determined after 24.0 h. of incubation at 37.0 ± 2 °C with first inoculums of 5×10^5 CFU/ml for bacteria, and 0.5–2.5 $\times$ 10^3 CFU/mL for yeast at 600 nm. MIC was defined by operating ELISA plate types within a wavelength of 600 nm.

Results and Discussion

Synthesis of AgNPs by Fluc. and Gamma Radiation

AgNPs are remarkably proficient at absorbing and distributing light and, unlike common dyes and pigments, produce a color that depends on the extent and the configuration of the produced NPs [1, 14, 20, 26, 33].

Table (S1) confirmed the synthesis of AgNPs through the reduction of aqueous Ag^+ solution (1.0, 1.5 and 2.0 mM) after mixing with Fluc. solution (1.0, 2.0, and 4.0 mg/mL) and exposure to different gamma radiation doses (1.0, 5.0, and 10.0 kGy) by measuring its optical Density (O.D.) using UV–Vis. spectroscopy.

Results in Table (S1) displays that, O.D. of AgNPs extends the peak intensities with contemporary blue shifts. This implies the production of AgNPs with superior yields with small sizes [34]. The powerful absorption band observed at 415.0 nm meant AgNPs production [16].

Our decisions reveal that, run no. 25 in Table (S1) including the optimized condition (1.5 mM $AgNO_3$, 2.0 mg/mL Fluc. and 5.0 kGy gamma-ray dose) records raised in the O.D (2.54) higher than additional runs, with increasing in AgNPs yield.

It is extremely recognized that, AgNPs show a deep brown appearance in aqueous solution due to the Surface Plasmon Resonance (SPR) of metal nanoparticles [16, 35].

Moreover, Fig. 1 displayed the progressive color difference from transparent (Fluc. and Ag^+) to cloudy brown color, indicating AgNPs synthesis.

An unusual feature of the synthesized AgNPs is that this SPR height wavelength can be attuned from 450.0 nm (violet light) to 550.0 nm (green light) by adjusting the particle extent and the local refractive index near the NPs surface. Also, extended shifts of the SPR peak wavelength down within the infrared area of the electromagnetic

Fig. 1 Gradual colour difference from colourless (Fluc. and Ag^+) to deep brown colour, indicating the production of AgNPs (Color figure online)

spectrum can be obtained by fabricating AgNPs with spherical shapes [1, 11, 20, 26, 30].

Mechanistic Design for Gamma Rays-Assisted Nucleation and Germination of AgNPs

Kinetic investigations of the reduction method explained that, the synthesis of AgNPs begins outwardly radiation; this reduction is remarkably enhanced by gamma irradiation particularly at 5.0 kGy, suggesting that radiation has significant capacity in the production of AgNPs [11, 14, 20, 27, 36, 37].

The radicals and electrons generated in water simultaneous gamma irradiation are e^-_{aq}, $OH^{\cdot}$, $H^{\cdot}$, H_2, and H_2O_2 (Eq. 1).

The success of gamma irradiation for the construction of AgNPs extends in the evidence that, wanted product of extremely reducing free electron without the creation of either byproduct [1, 11, 20].

The overall reaction reviewed the use of available electron as a reducing potential to Ag^+ ions and effectiveness of Fluc. as a stabilizer toward AgNPs development. The reaction was starting by the dissolving and hydrolysis of $AgNO_3$ to its ions Ag^+ and NO_3^- (Eq. 2). Following the asserted experimental situations, the conversion of Ag^+ takes place by electron removal from hydrated electrons to create zerovalent AgNPs (Eq. 3). The free radicals $OH^{\cdot}$ and $H^{\cdot}$ are competent to discharge hydrogen from the Fluc. generating a Fluc. radical (secondary radicals = $C_{13}H_{11}F_2N_6O^{\cdot}$; Eq. 4). Additionally, Fluc. radical was attack Ag^+ to form AgNPs and steady Fluc. building (Eq. 5). Finally, the stable Fluc. can preserve AgNPs by the incorporation and capping with it as conferred in Eq. 6.

$$H_2O \xrightarrow{\gamma\text{-ray (Radiolysis)}} e^-_{aq} + OH^{\cdot} + H^{\cdot} + H_2 + H_2O_2 \quad (1)$$

$$AgNO_3 + H_2O \xrightarrow{\text{Hydrolysis}} Ag^+ + NO_3^- \quad (2)$$

$$Ag^+ + e^-_{aq} \xrightarrow{\text{Reduction}} Ag^{\cdot} \quad (3)$$

$$C_{13}H_{12}F_2N_6O + OH^{\cdot} \rightarrow C_{13}H_{11}F_2N_6O^{\cdot} + H_2O \quad (4)$$

$$2C_{13}H_{11}F_2N_6O^{\cdot} + Ag^+ + H_2O \xrightarrow{\text{Reduction}} Ag^{\cdot} + [C_{13}H_{12}F_2N_6O]_2 + H_3O^+ \quad (5)$$

$$C_{13}H_{12}F_2N_6O + Ag^{\cdot} \xrightarrow{\text{Stabilization and capping}} [C_{13}H_{12}F_2N_6O]Ag^{\cdot} \quad (6)$$

Figure 2, introduced the scheme of Ag^+ reduction in solution by ionizing radiation in the presence of a stabilizer (Fluc.). Subsequently, the hydroxyl groups, nitrogen and fluoride atoms being in Fluc. ($C_{13}H_{12}F_2N_6O$) were covered and stabilized AgNPs, while hindering their excessive aggregates and agglomeration.

Characterization of AgNPs

UV–Vis. spectrophotometer was performed for the validation of the synthesized AgNPs. The UV–Vis. design was a simplistic, speedy, cost-effective, and occurred to obtain the investigation about AgNPs synthesis and incorporation [38, 39].

The colloidal suspension of AgNPs was presented especially, dark brown color; that prejudice of their low dimensionality, and Surface Plasmon Resonance (SPR) [2, 7, 12, 20, 26, 40]. Commonly, the SPR bands are controlled by the size, appearance, morphology, configuration and dielectric properties of NPs [41, 42].

As displayed in Fig. 3, UV–Vis. spectra of the aqueous Fluc. and AgNPs solutions synthesized at 5.0 kGy and in the absence of gamma doses (non-irradiated samples), the

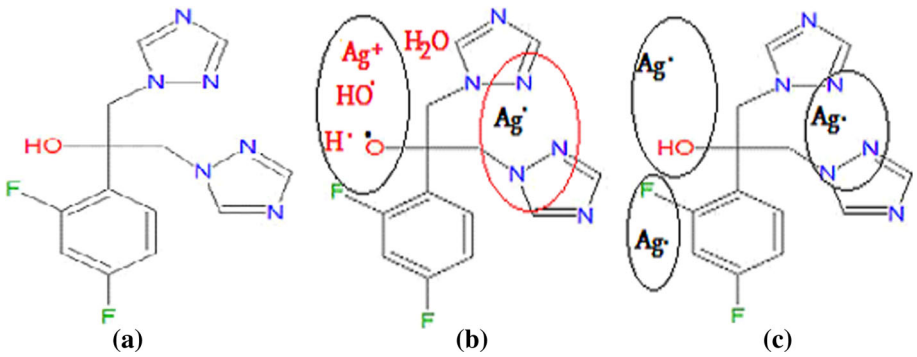

Fig. 2 Reduction steps in AgNPs synthesis where, **a** chemical structure of Fluc., **b** reduction and stabilization processes caused by Fluc., and **c** the complete stabilization of AgNPs by Fluc.

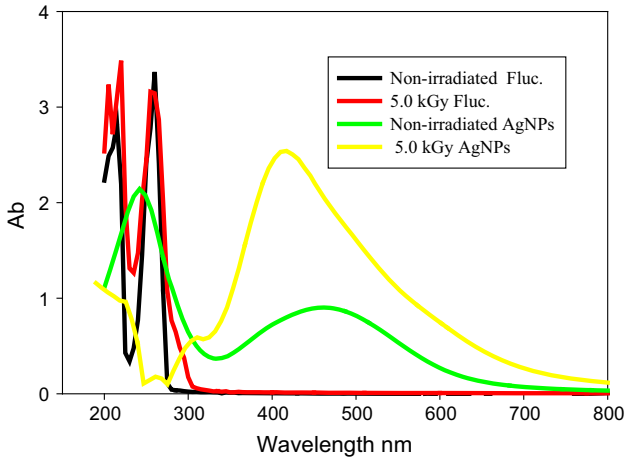

Fig. 3 UV–Vis. spectrum of the aqueous solutions of non-irradiated and irradiated (5.0 kGy) Fluc. and AgNPs

measuring being reported after achievement of the reaction.

The decision of UV–Vis. spectrum of AgNPs manufactured at 5.0 kGy sharply confers, an extraordinary SPR band at 410.0 nm simultaneously with raised O.D (2.54 Ab) higher than non-irradiated one with the sharp peak head. This meant the development of large yield and small size of AgNPs.

Consequently, the progression in the peaks intensity, were essentially owed to the production of further AgNPs [43, 44], that, implies substantial reduction potential of the Fluc. at 5.0 kGy. On the other hand, Fluc. peak was recognized at the spectrum from 210.0 to 260.0 nm [41]. Earlier investigations have revealed that, AgNPs present to the absorption band at nearly 400.0 to 550.0 nm in the UV–Visible spectra [45].

It should be noted that, no vital variations in the peak position or intensity of the SPR are recognized when Fluc. solution presented to 5.0 kGy in associate with non-irradiated one (Fig. 3), which implies the stability of Fluc. at 5.0 kGy.

The gradual formation and growth of AgNPs at different gamma rays doses (5.0, 10.0, 15.0, 20.0, 25.0, and 30.0 kGy) and constant condition ($AgNO_3$ Conc. 0.5, 1.5, 2.0 mM and Fluc. Conc. 1.0, 2.0, 4.0 mg/ml) were studied using UV–Vis spectroscopy as shown in Fig. 4.

Band features of AgNPs have identified nearby 415.0 nm (Fig. 4), which greatly recommends that AgNPs were rounded in shape and have been approved by the TEM image. For AgNPs solution (not agglomerated), the UV–Visible extinction spectra were practiced to quantify the concentration of AgNPs. Due to the direct relationship within O.D. and concentration, the values of O.D. may be applied to calculate its concentration [29]. Furthermore, the change in SPR peaks may be associated with the synthesis of AgNPs at various particle sizes [46].

The specific absorption highest peak of the synthesized AgNPs was constantly blue shafted from 415.0 nm (non-irradiated) to 450.0 nm (5.0 kGy) with the increase in the intensity.

This intimates that, as radiation was developed (up to 5.0 kGy), AgNPs yield were improved and reduced in the particle size. The broadness of the SPR peak also declined, with rising radiation doses, registering NPs with small size configuration.

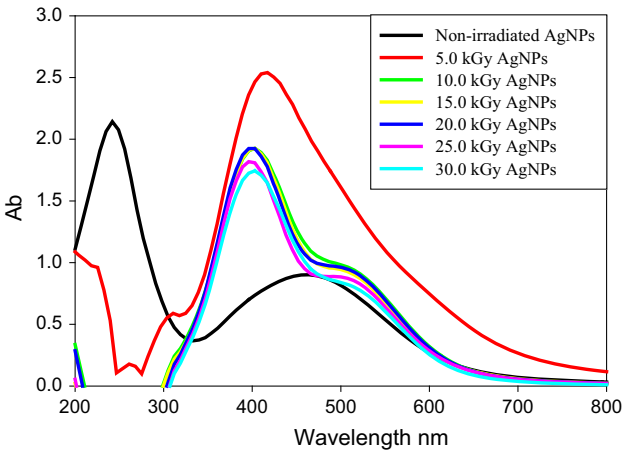

Fig. 4 Synthesis of AgNPs by Fluc. at different gamma irradiation doses (5.0, 10.0, 15.0, 20.0, 25.0, and 30.0 kGy) and at room temperature

The regular development in AgNPs growth and reductions in O.D. at varying radiation doses extended from 5.0 to 30.0 kGy with fixed condition (1.5 mM $AgNO_3$ Conc., and 2.0 mg/mL Fluc. Conc.), were examined using UV–Vis. spectroscopy (Fig. 4).

Additionally, the development of irradiation doses from 5.0 to 30.0 kGy, explains the drop in the corresponding peak intensities. It was assigned to the reduction in AgNPs synthesis and agglomeration had been recorded.

AgNPs produced by gamma radiation direct to combine into oligomers, which themselves strongly develop toward massive clusters [12]. Though, the coalescence needs to be defined by restricted radiation treatment to keep particles serving as a clump stabilizer. Functional groups including the special relationship to the metal secure the anchoring of the fragment at the group cover while preserves the cluster from combining among the following unity by the satiric barrier or electrostatic repulsion [39].

So, Fluc. was chosen as a capping and stabilizer tool for AgNPs stabilization, these capacity limited by increasing gamma rays treatments that, direct to the agglomeration and the precipitation of the synthesized AgNPs.

To examine the distribution of AgNPs particles size, DLS was conducted, and its results were associated with the TEM image [1, 20]. The average particle size was determined by DLS method and was defined as 13.30 nm in AgNPs synthesized by Fluc. and gamma radiated at 5.0 kGy as showed in Fig. 5.

Moreover, TEM image established the spherical shapes of AgNPs in nanoscale from 7.30 to 18.25 nm with the average mean diameter of 11.65 nm as displayed in Fig. 6.

The size of AgNPs received from DLS analysis (13.30 nm) was larger than the TEM image (11.65 nm), because DLS analysis was involved the hydrodynamic radius, which brings into consideration all the Fluc. seems not receive in the reduction process [1, 12, 20].

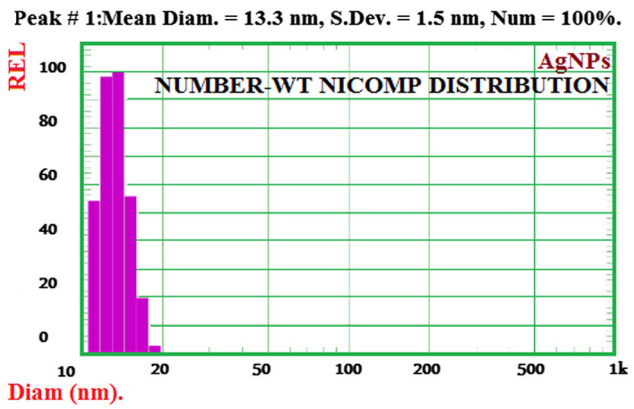

Fig. 5 DLS of AgNPs synthesized by Fluc. and gamma irradiation at 5.0 kGy

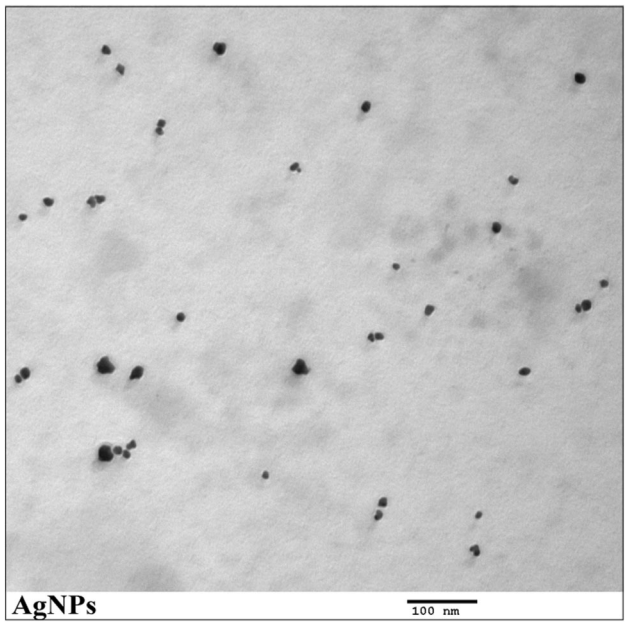

Fig. 6 TEM image of AgNPs synthesized by Fluc. and gamma irradiation at 5.0 kGy

XRD presents a real analysis of the composition and the arrangement of the identified NPs because it awards size, axes, and the station of the atoms [2, 13, 47, 48].

XRD pattern to the AgNPs was presented in Fig. 7; many peaks were observed, those for AgNPs. Diffraction characteristics are showing within 2θ (degree) as 38.13°, 44.21°, 64.47°, and 77.37° where these peaks describe the Bragg's reflections (111), (200), (220) and (311) planes in that order respectively. This indicates the face-centered cubic (fcc) crystalline composition of AgNPs [26].

Dropping off a peak at 31.3°, 32.6°, and 33.6° implies that, the manufactured AgNPs are clear and freed from silver oxide NPs [49].

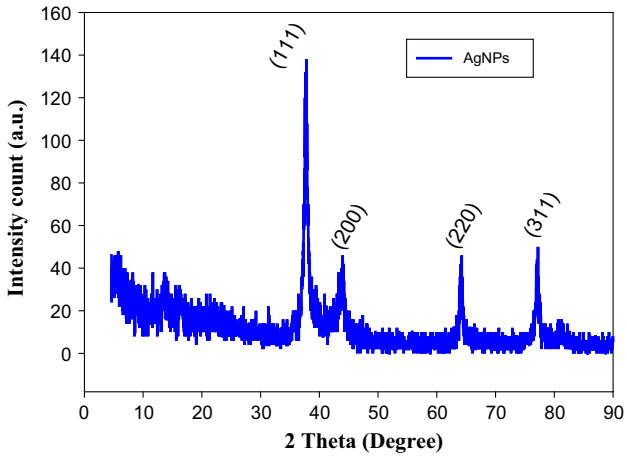

Fig. 7 XRD of AgNPs synthesized by Fluc. and gamma irradiation at 5.0 kGy

The results of FTIR spectrum of non-irradiated Fluc., Fluc. irradiated at 5.0 kGy, AgNPs synthesized by Fluc. at room temperature (non-irradiated), and AgNPs synthesized by Fluc. at 5.0 kGy were displayed in Fig. 8, and illustrated in Table 2.

It was found from Fig. 8 and Table 1 that, there were slight changes in T% between both irradiated and non-irradiated Fluc. On the other hand, there were no differences between the wave-number of both Fluc., suggested that, the Fluc. structure not breakdown under the effect of gamma rays and still stable even after exposure.

Additionally, by making comparison between FTIR spectrums of both irradiated Fluc. at 5.0 kGy and AgNPs synthesized by Fluc. at 5.0 kGy, there were no changes in all peaks position, but some slightly T% changes had been detected. These changes in T% may be attributed to the incorporation of the synthesized AgNPs with its stabilizer Fluc. in the active sites by physical bond (Van Der Waals forces) [1, 20, 50].

By implementing a relationship within FT-IR spectrums of AgNPs synthesized by Fluc. (Irradiated; yellow line), the differences over the bands of the Fluc. (Irradiated; red line), may be connected with the changing of the force constant (k) of the Fluc. units due to the adsorption of the hydroxyl groups, nitrogen and fluoride atoms of Fluc. upon the AgNPs as explained in Eq. (7).

$$\upsilon = \frac{1}{2\pi}\sqrt{\frac{k}{\mu}} \tag{7}$$

The changing in peaks was associated to triazole group, 2, 4-Difluorobenzyl group, and propane backbone positively verified that, the derived Fluc. reduces silver nitrate.

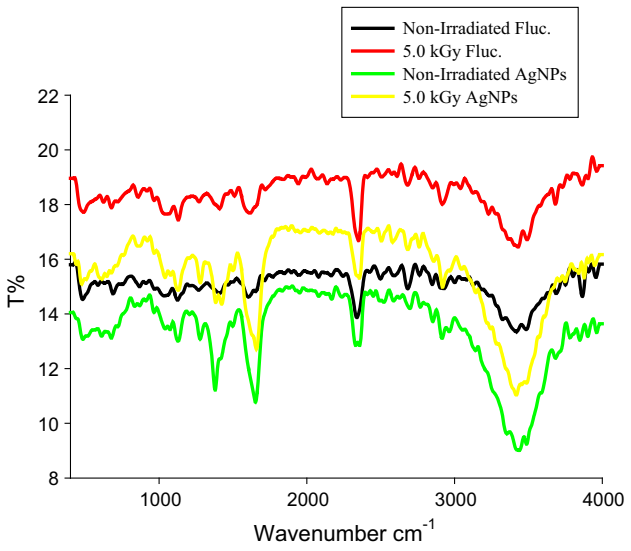

Fig. 8 FTIR spectrum of non-irradiated and irradiated (5.0 kGy) Fluc. and AgNPs

At the same time, Fluc. was preserved AgNPs from agglomeration and further prevent deactivation [2].

It described briefly that, Fluc. could connect to AgNPs either by amide groups or by the electrostatic affinity of negatively charged hydroxyl groups [51], and consequently, preserve, and prevent AgNPs from precipitation and aggregation.

Antimicrobial Activity of the Synthesized AgNPs

The unique features of inorganic nanoparticles are their large surface to volume ratio and their nano-scale size, which enhance the response beside pathogenic microorganisms [52].

AgNPs (75.0 µg/mL) incorporated by Fluc. at 5.0 kGy, were presented a successful impact as antibacterial factors towards MDR bacteria, including the promising action against *A. baumannii* (20.0 mm ZOI), followed by *E. faecalis* (19.0 mm ZOI) as recorded in Table 2. On the other hand, it was revealed a maximal growth repression against the standard ATTC bacteria including *P. aeruginosa* ATCC 27853 (18.0 mm ZOI), followed by *E. coli* ATCC 25922 (17.0 mm ZOI).

Positively, our manufactured AgNPs was an encouraging anti-TB toward *M. tuberculosis* RCMB 010126 (12.0 mm ZOI), that compared with a standard AMC used (9.0 mm ZOI). Additionally, all tested bacterial pathogen was resistance to Fluc., and the tested MDR bacteria were also resistance to the standard antibiotic AMC.

From our results illustrated in Table 2, it necessity consider that AgNPs synthesized by Fluc. at 5.0 kGy were further active upon unicellular fungi *C. albicans* ATCC 10231 (17.0 mm ZOI), where Fluc. (1000 ppm) alone, hinder its growth by 9.0 mm ZOI, and standard Nystatin by 8.0 mm ZOI. From the last mentioned antifungal results, we interoperated that, AgNPs incorporated by Fluc. at 5.0 kGy, were proposed a synergistic impact upon *C. albicans.*

The synergistic result obtained due to the performance of AgNPs and its reducer and stabilizer Fluc., but the antibacterial activity against all tested bacteria was because of AgNPs entirely, and the principal characters of Fluc., were reduced and preserved AgNPs from agglomeration.

Our results achieved in Table 2 revealed that, $AgNO_3$ produced smaller ZOI as correlated to AgNPs at the related concentration recommended a powerful antibacterial action is expected to AgNPs. Aforementioned, it can be due to reduction of $AgNO_3$ into AgNPs which ended an extended surface area and great penetration of AgNPs that drive to excellent surface association with bacteria and hence greater in the bactericidal action [53].

The MIC results of AgNPs (Table 3) against the standard ATTC bacteria, MDR bacteria, *M. tuberculosis*, and

Table 1 FT-IR spectrum of non-irradiated Fluc., Fluc. irradiated at 5.0 kGy, AgNPs synthesized by Fluc. at room temperature (non-irradiated), and AgNPs synthesized by Fluc. at 5.0 kGy and its corresponding assignment

Non-irradiated Fluc. (black line) wave-number (cm^{-1})	Irradiated Fluc. (5.0 kGy) (red line) wave-number (cm^{-1})	AgNPs synthesized by Fluc. at room temp (green line) wave-number (cm^{-1})	AgNPs synthesized by Fluc. at 5.0 kGy (yellow line) wave-number (cm^{-1})	Assignment
Triazole group				
3430.12	3443.28	3430.12	3423.29	CH stretch
1386.41	1399.31	1372.97	1389.21	Ring stretch
1241.29	1257.36	1267.63	1267.12	Ring stretch
1122.78	1121.54	1122.12	1125.21	Ring breath
845.51	872.58	872.45	872.12	Ring bend
2,4-Difluorobenzyl group				
3056.05	3035.81	3035.81	3046.05	CH stretch
1603.41	1623.90	1653.65	1653.89	C=C stretch
1267.63	1267.63	1277.87	1277.87	CF stretch
1044.50	1024.02	1024.02	1024.02	CH deform
Propane backbone				
2913.64	2903.39	2903.39	2913.64	CH_2 stretch
1410.28	1410.28	1420.52	1420.52	CH_2 scissor
1125.71	1125.71	1125.71	1125.71	C–C stretch
1075.23	1075.21	1084.74	1075.23	C-(OH) stretch

the unicellular fungi remained in the range of 1.172–18.72 μg/mL.

Although AgNPs established the MIC value of 1.172 μg/mL against *A. baumannii* in the MDR bacteria, it was confirmed the MIC values of 2.343 μg/mL toward *P. aeruginosa* in the standard ATTC bacteria and 4.687 μg/mL upon *C. albicans*. On the other hand, the MIC of Fluc. alone was 250 μg/mL against *C. albicans*.

The diameter of ZOI describes the magnitude of sensitivity of microbes [2]. It must mentioned that, Gram-positive bacteria revealed a tremendous repression zone than Gram-negative bacteria; that suggests Gram-positive bacteria were further susceptible to AgNPs compared with the Gram-negative bacteria in all examined strains. The same determination of antimicrobial action has been managed with BiONPs, CuONPs, and ZnNPs [2, 12, 13, 54].

In this paper, we should extend compelling evidence of the efficiency of AgNPs synthesized by Fluc. at 5.0 kGy to control MDR bacteria, standard ATTC bacteria, and pathogenic *C. albicans*. Moreover, AgNPs have the potential to inhibit bacterial and fungal prolongation which was higher than standard antibiotics used (AMC and Nystatin).

Related articles would be defined the purpose of AgNPs as antibacterial agent superimposed pathogenic bacteria. Balaram et al. [55], regarded the action of AgNPs manufactured by green biological systems, and was observed to be effective upon MDR *E. coli* strain (8.0 mm ZOI; 4.0 μg/mL MIC), and MDR *S. aureus* strain (10.0 mm ZOI; 8.0 μg/mL MIC).

On the other hand, Juhi et al. [56], integrated and optimized green AgNPs (75.0 ppm) and studied its action upon *E. coli* (15.0 mm ZOI), and *S. aureus* (14.0 mm ZOI), and consider the influence of Ag^+ against *E. coli* (11.0 mm ZOI), and *S. aureus* (12.0 mm ZOI).

Additionally, Anbarasan et al. [57], presented saponin-conjugated AgNPs and study its antibacterial action upon remarkable decided pathogenic bacteria, and was observed to be lethal for *E. faecalis*, *S. aureus*, *E. cloacae*, *E. coli*, *K. pneumoniae*, *P. aeruginosa*, *A. baumannii*, *E. asburiae*, *E. kobei*, and *Proteus mirabilis* by 9.0, 10.0, 8.5, 8.0, 9.0, 7.0, 8.0, 10.0, 9.5, and 7.5 mm ZOI sequentially, while both controls (saponin and Ag^+) doesn't produce any activity upon the examined bacteria.

Besides, Rupak et al. [58], studied the antimicrobial activity of enzyme-mediated AgNPs (20 μL) formulation that overcame the microbial growth of *E. coli*, *S. pneumoniae*, *K. pneumoniae*, *S. aureus*, *P. aeruginosa*, *B. cereus*, *B. subtilis*, and *C. albicans* by 12.66, 14.33, 14.16, 15.0, 15.5, 12.5, 16.0, and 12.0 mm ZOI respectively, and

Table 2 Antibacterial and antifungal activities of AgNPs synthesized by Fluc. and gamma irradiated at 5.0 kGy, Fluc. alone, and Ag^+ against some standard strains (ATCC&RCMB), multidrug-resistant bacteria, and unicellular fungi as ZOI (mm)

Microbial pathogens	ZOI of AgNPs (75.0 ppm) synthesized by Fluc. (1000 ppm) at 5.0 kGy (mm)	ZOI of Fluc. (1000 ppm) (nm)	ZOI of Ag^+ ion (75.0 ppm) (nm)	AMC; 20/10 µg/mL and NS; 100 µg/mL
Standard strains (ATCC) and (RCMB)				
Bacillus subtilis ATCC 6633	$15.0^{cd} \pm 0.57735$	Negative	$8.0^{de} \pm 0.76376$	$12.0^{bc} \pm 0.50000$
Klebsiella pneumoniae ATCC 4352	$10.0^{a} \pm 1.00000$	Negative	$8.0^{f} \pm 0.57735$	$9.0^{a} \pm 0.57735$
Pseudomonas aeruginosa ATCC 27853	$18.0^{e} \pm 0.57735$	Negative	$7.0^{ef} \pm 1.15470$	$10.0^{b} \pm 1.15470$
Enterococcus faecalis ATCC 29212	$14.0^{c} \pm 0.57735$	Negative	$7.0^{de} \pm 0.57735$	$12.0^{bc} \pm 1.00000$
Escherichia coli ATCC 25922	$17.0^{d} \pm 1.00000$	Negative	$11.0^{de} \pm 1.15470$	$14.0^{d} \pm 0.28868$
Staphylococcus aureus ATCC 29213	$15.0^{c} \pm 1.00000$	Negative	$8.0^{de} \pm 1.00000$	$13.0^{c} \pm 1.15470$
Mycobacterium tuberculosis RCMB 010126	$12.0^{b} \pm 0.57735$	Negative	$7.0^{de} \pm 1.52753$	$9.0^{a} \pm 0.57735$
Multidrug-resistant bacteria				
Staphylococcus aureus (MRSA)	$12.0^{b} \pm 0.57735$	Negative	$7.0^{ef} \pm 1.15470$	Negative
Staphylococcus epidermidis	$15.0^{c} \pm 1.00000$	Negative	$8.0^{d} \pm 0.57735$	Negative
Acinetobacter baumannii	$20.0^{f} \pm 1.00000$	Negative	$9.0^{c} \pm 1.00000$	Negative
Escherichia coli	$13.0^{c} \pm 1.00000$	Negative	$8.0^{f} \pm 0.57735$	Negative
Enterococcus faecalis	$19.0^{e} \pm 0.57735$	Negative	$12.0^{f} \pm 1.00000$	Negative
Enterobacter cloacae	$14.0^{c} \pm 1.00000$	Negative	$9.0^{b} \pm 0.57735$	Negative
Unicellular fungi				
Candida albicans ATCC 10231	$17.0^{c} \pm 0.57735$	9.0 ± 1.00000	$8.0^{a} \pm 1.00000$	$8.0^{a} \pm 0.57735$
LSD	1.66667	–	1.66667	1.50000

Values are mean ± SD (n = 3). Data within the groups are analyzed using one-way analysis of variance (ANOVA) followed by Duncan's multiple range test (DMRT), LSD, least significant differences

Negative means that no ZOI had been measured

AMC, amoxicillin/clavulanic acid (antibacterial standard)

NS, nystatin (antifungal standard)

$^{a, b, c, d, e, f}$Duncan's multiple range test at $p < 0.05$

the Ag^+ was less effective than AgNPs in all tested microbes.

Eventually, Afreen et al. [59], were studied the antibacterial action (Microplate Alamar Blue Assay) of AgNPs integrated from enzyme (extracted from *R. stolonifer*) upon clinical isolates of *M. tuberculosis*. The results registered that, all clinical isolates were restrained within the MIC range of 6.25–12.5 µg/mL of AgNPs.

The antimicrobial efficiency of AgNPs was estimated by several researchers toward a broad spectrum of microbes, involves MDR and non-MDR strains of bacteria, viruses, and fungi. Metal NPs are presently fully-established as an encouraging alternative to antibiotic treatment because they own incredible potential for resolving the difficulty connected with the increase of MDR in pathogenic microbes, therefore, they are considered as next-generation antibiotics [60]. Inappropriate, the application of AgNPs has achieved much recognition in this interest [61–63].

Action Mechanism of AgNPs Upon Microbial Cell

AgNPs have been showing sufficient activity upon beyond 650 microbes like bacteria (both Gram-positive and negative), fungi and viruses; the exact mechanism of their form of antimicrobial behavior is not completely explained yet [64]. Some primary investigated forms of an antimicrobial performance of AgNPs have been identified (Fig. 9 and Table 4). The antimicrobial performance of AgNPs is associated with four completely-defined mechanisms.

The first one described the adhesion of AgNPs over the outside of cell wall and membrane, it occurred because the positive charge presents electrostatic affinity within AgNPs and negatively charged cell membrane of bacteria, through promotes AgNPs attachment over cell membranes. Morphological differences display visible in such interaction and can be identified by decrease of the cytoplasm and membrane organization eventually starting to crack of the bacterial cell wall [65].

Table 3 Antibacterial and antifungal activities of AgNPs synthesized by Fluc. and gamma irradiated at 5.0 kGy, Fluc. alone, and Ag^+ against some standard strains (ATCC&RCMB), multidrug-resistant bacteria, and unicellular fungi as MIC (μg/mL)

Microbial pathogens	MIC of AgNPs (75.0 ppm) synthesized by Fluc. (1000 ppm) at 5.0 kGy (μg/mL)	MIC of Fluc. (1000 ppm) (μg/mL)	MIC of Ag^+ ion (75.0 ppm) (μg/mL)
Standard strains (ATCC) and (RCMB)			
Bacillus subtilis ATCC 6633	$4.68^{ab} \pm 0.76376$	Negative	$75.00^{ab} \pm 0.76376$
Klebsiella pneumoniae ATCC 4352	$18.75^{c} \pm 0.57735$	Negative	$75.00^{d} \pm 0.57735$
Pseudomonas aeruginosa ATCC 27853	$2.34^{d} \pm 0.28868$	Negative	$75.00^{c} \pm 0.28868$
Enterococcus faecalis ATCC 29212	$9.37^{a} \pm 0.76376$	Negative	$75.00^{cd} \pm 0.76376$
Escherichia coli ATCC 25922	$4.68^{d} \pm 0.76376$	Negative	$37.50^{a} \pm 0.76376$
Staphylococcus aureus ATCC 29213	$4.68^{a} \pm 0.76376$	Negative	$37.50^{a} \pm 0.76376$
Mycobacterium tuberculosis RCMB 010126	$9.37^{ab} \pm 0.76376$	Negative	$75.0^{ab} \pm 0.76376$
Multidrug-resistant bacteria			
Staphylococcus aureus (MRSA)	$9.37^{c} \pm 1.00000$	Negative	$75.00^{a} \pm 1.00000$
Staphylococcus epidermidis	$4.68^{ac} \pm 0.28868$	Negative	$75.00^{c} \pm 0.28868$
Acinetobacter baumannii	$1.17^{b} \pm 0.57735$	Negative	$37.50^{c} \pm 0.57735$
Escherichia coli	$9.37^{d} \pm 0.57735$	Negative	$18.75^{d} \pm 0.57735$
Enterococcus faecalis	$1.17^{d} \pm 1.00000$	Negative	$9.375^{b} \pm 1.00000$
Enterobacter cloacae	$9.37^{a} \pm 1.00000$	Negative	$18.75^{a} \pm 1.00000$
Unicellular fungi			
Candida albicans ATCC 10231	$4.68^{a} \pm 1.15470$	250 ± 1.00000	$18.75^{ab} \pm 1.15470$
LSD	1.33333	–	1.66667

Values are mean ± SD (n = 3). Data within the groups are analyzed using one-way analysis of variance (ANOVA) followed by Duncan's multiple range test (DMRT), LSD, least significant differences

Negative means no activity had been detected

[a, b, c, d]Duncan's multiple range test at $p < 0.05$

Besides electrostatic performance, the interaction between AgNPs and sulfur-containing proteins being in the cell wall produces irreversible alterations in cell wall composition occurring in its splitting [66]. This, in turn, influences the integrity of lipid bilayer and permeability of the cell membrane. The modifications in cell morphology produce an improvement in layer permeability, which changes cells capacity to accurately control transportation within the plasma membrane [67].

For example, silver reduces the uptake and discharge of phosphate anion in *E. coli* [67]. Furthermore, Ag^+ can also decay carrier and the liberation of potassium (K^+) cation from the microbial cells. Besides changing the conveyor movement, the improvement in membrane permeability may become further declared results such as failure by leakage of cellular contents, including proteins, cations, anions, reducing sugars and the cellular power storage (ATP) [68–70].

While, the secondary mechanism was examined the perception of AgNPs inside the cell and breaking of intracellular composition (vacuoles, mitochondria, ribosomes) and biomolecules (lipids, protein, and DNA). Cooperation with cellular arrangements and biomolecules has particularly damaging results against microbes. Inappropriate, AgNPs interaction with ribosomes leads to their denaturation producing repression of protein synthesis and translation [60, 71, 72].

It must be noted that, Ag^+ may deactivate the proteins by combine with the working groups of its. For example, Ag^+ quandary to thiol groups (ASH) of the protein found in the cell layer creating permanent SA-Ag connections appears in protein denaturation [60, 73].

The proteins are required in transmembrane ATP production and improving ion transportation beyond cell membrane [73]. Both AgNPs and Ag^+ reconstruct the 3D arrangement of proteins by the interaction and conflict with disulfide links and hinder effective binding positions driving to overall operative errors in the microbes [68]. Furthermore, The interaction of AgNPs with DNA may produce denaturation regarding the DNA and delay in cell replication [74].

The third mechanism explained that, AgNPs caused cellular toxicity and oxidative tension created by production of Reactive Oxygen Species (ROS) and free radicals [69, 75]. The formation of ROS in microbial cells induces cell destruction, although, the exact mechanism of ROS-

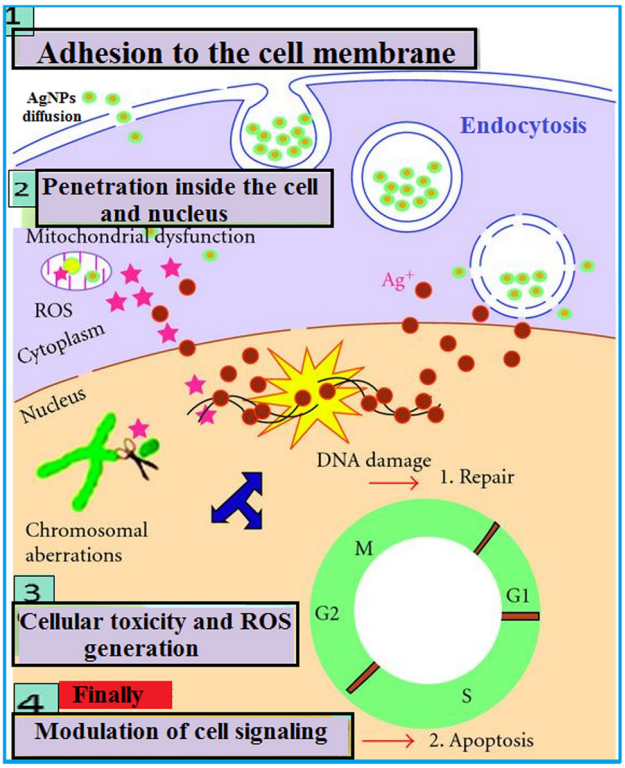

Fig. 9 The four most prominent routes of antimicrobial action of AgNPs, where [1] AgNPs adhere to microbial cell surface and results in membrane damage and altered transport activity; [2] AgNPs penetrate inside the microbial cells and interact with cellular organelles and bio-molecules, and thereby, affect respective cellular machinery; [3] AgNPs cause increase in ROS inside the microbial cells leading to cell damage and; [4] AgNPs modulate cellular signal system ultimately causing cell death

generated antibacterial movement of AgNPs is not wholly cleared [76].

This deadly influence may be due to the adhesive of Ag^+ over the cell membrane, which consequently transfers warning and prevents the mitochondrial respiratory capacity of the bacteria [77]. Ag^+ is identified beginning dysfunction of respiratory electron transportation series by separating it from oxidative phosphorylation by restraining respiratory succession enzymes [78]. The extreme significance of created free radical purposes straight injury to mitochondrial membrane generating decay, and finally, cell destruction.

AgNPs produced genotoxicity involves chromosomal irregularities such as modifications, oxidative DNA base destruction, and DNA strand separations [79].

Lastly, the immediate mechanism described that AgNPs effects signal transduction modulation pathways. Phosphorylation of different protein substrates in bacteria is generally understood [80]. The sequence of phosphorylation and de-phosphorylation is tool of sign relays in microbes necessary for microbial majority and cellular movement [81].

Accordingly, repression of phosphorylation of proteins would hinder their enzymatic action, which will affect in hindrance of bacterial germination. AgNPs changes cellular signaling and performances by dephosphorylating deposits on essential microbial peptide substances and thus repress microbial majority [82].

Besides, those four fully-recognized mechanisms, AgNPs also induce the immune system of the human cells by arranging incendiary reply, which additional support in restraint of the microbes [83].

Whereas AgNPs do not significantly exercise linear particle-specific toxicity on microbes, AgNPs could be directed to various particle compositions (e.g., exterior coverings) to deliver Ag^+ at wanted speed and position. Moreover, AgNPs may work as a carrier to release Ag^+ more completely (meaning less sensitive to coupling and decreased bioavailability by popular simple ligands [84]) to the bacterial membrane, and cytoplasm (Fig. 10), whose proton motive power would lower the district pH (as below as pH 3.5) [85], and improve Ag^+ discharge.

Additionally, AgNPs were performance as powerful antifungal means by invading fungal layers, thus obstructing fungal membrane. In common, fluconazole connects to layer sterols and transmembrane holes are created, thus creating a leakage of cell components and ultimately cell loss [86]. Here, certain data were practiced to evaluate the global rigidity of the plasma membrane within the difference among AgNPs and fluconazole.

Considering the individual preservation of intracellular elements is significant to cell viability, the trehalose and glucose may denote identity of various intracellular ingredients released through layer separation after AgNPs penetration [87].

Trehalose can defend proteins and natural layers from denaturation induced by a mixture of stress situations, involving dehydration, energy, desiccation, freezing, oxidation, and lethal factors in fungi [88].

From our encourage results, we can attend that, Fluc. designed novel approaches for the assembly and stabilization of AgNPs in the presence of gamma rays, which in turn recommended the practice of alternative modes (green techniques) rather than the chemical processes which produced the risk and hazardous for the environment.

The designed AgNPs can apply as the disinfectant factors that maintains a novel and a powerful antimicrobial activity against a broad variety of pathogenic microbes. After considering its toxicity level, AgNPs needs to implement in all medical, pathological, industrial, agricultural, and pharmaceutical purposes.

Table 4 Mode of antimicrobial action of AgNPs against some tested bacteria

Bacterial strains	Mode of action
Gram-positive	
Bacillus subtilis	Cell membrane damage; leakage of reducing sugars
	Degradation of chromosomal DNA; increase in ROS levels
Staphylococcus aureus	Adhesion to cell wall; cell membrane detachment from cell wall; DNA condensation; inhibition of replication; inactivation of proteins
	Cell membrane damage; leakage of reducing sugars
	Interaction with cell membrane; interaction with S- and P containing compounds; inhibition of respiration
Gram-negative	
Escherichia coli	Interaction with cell membrane; interaction with S- and P containing compounds; inhibition of respiration
	Adhesion to cell wall; cell membrane detachment from cell wall; DNA condensation; inhibition of replication; inactivation of proteins
	Cell membrane damage; leakage of reducing sugars
	Interaction with cell membrane; increase in membrane permeability; improper transport activity; leakage of cellular components
	Destabilization of ribosomes; inhibition of protein synthesis inhibition of expression of enzymes required for ATP generation
Klebsiella pneumonia	Interaction with DNA; inhibition of cell division
Pseudomonas aeruginosa	Interaction with cell membrane; interaction with S- and P containing compounds
	Penetration inside the cell
	Attenuation of quorum sensing

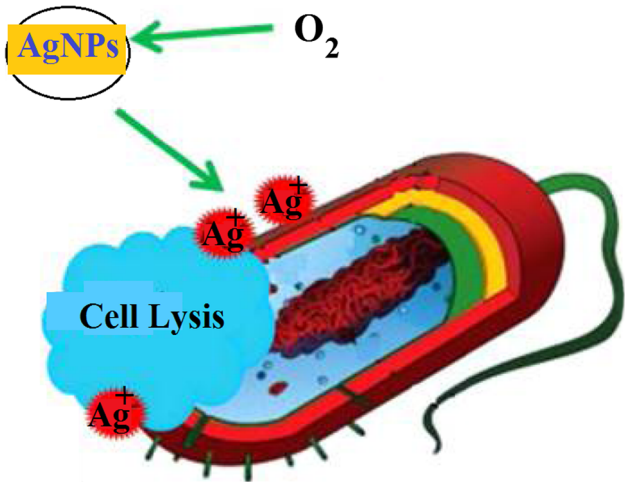

Fig. 10 Schematic of AgNPs, Ag^+, and cell interactions, where, AgNPs may serve as a vehicle to deliver Ag^+ more effectively to the bacteria cytoplasm and membrane, whose proton motive force would decrease the local pH (as low as pH 3.0) and enhance Ag^+ release

Conclusion

In summary, from our opinion, this research introduces the alternative method for AgNPs synthesis through the use of antifungal Fluc. The characterization technique investigates the shape and size of the synthesized AgNPs, which founded to be spherical with average size 11.56 nm. Antimicrobial studies as ZOI and MIC explained the synergistic effect between Fluc. and AgNPs as antifungal agents, while AgNPs were active against all tested pathogenic bacteria. Four investigated action mechanisms for the antimicrobial activity of AgNPs had been discussed. Gamma irradiation methods are clean, non-toxic technique, which used for metal NPs synthesis.

Acknowledgements The authors would like to thank the Nanotechnology Research Unit (P. I. Prof. Dr. Ahmed I. El-Batal), Drug Microbiology Lab., Drug Radiation Research Department, NCRRT, Egypt, for financing and supporting this study under the project "Nutraceuticals and Functional Foods Production by using Nano/Biotechnological and Irradiation Processes".

Compliance with Ethical Standards

Conflict of interest The authors declare that they have no conflict of interest.

Ethical Statement This article does not contain any studies with human participants or animals performed by any of the authors.

References

1. A. F. El-Baz, et al. (2016). *J. Basic Microbiol.* **56**, 531–540.
2. A. I. El-Batal, et al. (2017). *J. Photochem. Photobiol. B* **173**, 120–139.
3. G. Benelli (2017). *J. Clust. Sci.* **28**, (1), 11–14.

4. G. Benelli and M. Govindarajan (2017). *J. Clust. Sci.* **28**, (1), 287–308.
5. G. Benelli and C. M. Lukehart (2017). *J. Clust. Sci.* **28**, (1), 1–2.
6. S. Iravani, et al. (2014). *Res. Pharm. Sci.* **9**, (6), 385.
7. K. Gopinath, et al. (2017). *J. Clust. Sci.* **28**, (3), 1541–1550.
8. M. Govindarajan, M. Nicoletti, and G. Benelli (2016). *J. Clust. Sci.* **27**, 745–761.
9. J. M. Khaled, et al. (2017). *J. Clust. Sci.* **28**, (5), 3009–3019.
10. J. Li, et al. (2012). *Micro Nano Lett.* **7**, (4), 360–362.
11. A. El-Batal, et al. (2013). *World Appl. Sci. J.* **22**, (1), 01–16.
12. A. I. El-Batal, et al. (2017). *J. Clust. Sci.* **28**, (3), 1083–1112.
13. A. I. El-Batal, et al. (2017). *Int. J. Biol. Macromol.* **107**, 2298–2311.
14. A. El-Batal, et al. (2013). *J. Chem. Pharm. Res.* **5**, (8), 1–15.
15. M. A. El-Ghazaly, et al. (2016). *Can. J. Physiol. Pharmacol.* **95**, (2), 101–110.
16. M. Składanowski, et al. (2017). *J. Clust. Sci.* **28**, (1), 59–79.
17. R. R. Banala, V. B. Nagati, and P. R. Karnati (2015). *Saudi J. Biol. Sci.* **22**, (5), 637–644.
18. W. Schreiber, et al. (2003). *Invest Ophthalmol Vis Sci* **44**, (6), 2634–2643.
19. M. Ghorab and A. El-Batal (2002). *Boll. Chim. Farm.* **141**, (2), 110–117.
20. A. I. El-Batal, et al. (2014). *Br. J. Pharm. Res.* **4**, (11), 1341–1363.
21. V. Karthika, et al. (2017). *J. Photochem. Photobiol. B* **167**, 189–199.
22. M. Howarth, et al. (2005). *Proc. Natl. Acad. Sci. USA* **102**, (21), 7583–7588.
23. A. I. El-Batal and Mona Tamie (2015). *J. Chem. Pharm. Res.* **7**, 1020–1036.
24. A. I. El-Batal, et al. (2012). *World Appl. Sci. J.* **19**, (7), 962–971.
25. R. Jagannathan, P. Poddar, and A. Prabhune (2007). *J. Phys. Chem. C* **111**, (19), 6933–6938.
26. A. Baraka, et al. (2017). *Chem. Pap.* **71**, (11), 2271–2281.
27. A. El-Batal, et al. (2016). *J. Chem. Pharm. Res.* **8**, (4), 934–951.
28. A. I. El-Batal, et al. (2015). *Biotechnol. Rep.* **5**, 31–39.
29. M. Ghorab, et al. (2016). *Br. Biotechnol. J.* **16**, (1), 1–25.
30. A. El-Batal, et al. (2014). *Br. J. Pharm. Res.* **4**, (21), 2525–2547.
31. A. I. El-Batal, A.-A. M. Hashem, and N. M. Abdelbaky (2013). *SpringerPlus* **2**, (1), 129.
32. G. Funke, et al. (1998). *J. Clin. Microbiol.* **36**, (7), 1948–1952.
33. P. Venkatachalam, et al. (2017). *J. Clust. Sci.* **28**, (1), 607–619.
34. F.-K. Liu, et al. (2007). *Mater. Lett.* **61**, (11), 2402–2405.
35. S. Link and M. A. El-Sayed (2003). *Annu. Rev. Phys. Chem.* **54**, (1), 331–366.
36. A. I. El-Batal and M. S. Al Tamie (2016). *Pharm. Lett.* **8**, (2), 315–333.
37. N. M. Abdelbaky, *Cairo University Theses* (2012).
38. S. Naveed and M. Nafees (2015). *Open Access Libr. J.* **2**, (4), 1.
39. A. Hanora, et al. (2016). *J. Chem. Pharm. Res.* **8**, (3), 405–423.
40. A. I. El-Batal, et al. (2016). *Nanomater. Nanotechnol.* **6**, 13.
41. P. Sadasivudu, N. Shastri, and M. Sadanandam (2009). *Int. J. ChemTech Res.* **1**, (4), 1131–1136.
42. A. I. El-Batal, et al. (2018). *Microbial Pathog.* **118**, 159–169.
43. H. Bar, et al. (2009). *Colloids Surf. A Physicochem. Eng. Asp.* **339**, (1), 134–139.
44. H. Huang and X. Yang (2004). *Carbohydr. Res.* **339**, (15), 2627–2631.
45. K. G. Stamplecoskie and J. C. Scaiano (2010). *J. Am. Chem. Soc.* **132**, (6), 1825–1827.
46. S. Mohan, et al. (2014). *Carbohydr. Polym.* **106**, 469–474.
47. A. El-Batal, et al. (2014). *Br. J. Pharm. Res.* **4**(21).
48. A. El-Batal, et al. (2012). *Int. J. Pharm. Sci. Health Care* **6**, (2), 1–22.
49. A. Gannoruwa, B. Ariyasinghe, and J. Bandara (2016). *Catal. Sci. Technol.* **6**, (2), 479–487.
50. A. I. El-Batal, et al. (2016). *Bioengineering* **3**, (2), 14.
51. L. Rastogi and J. Arunachalam (2011). *Mater. Chem. Phys.* **129**, (1), 558–563.
52. Z.-M. Xiu, et al. (2012). *Nano Lett.* **12**, (8), 4271–4275.
53. S. Prabhu and E. K. Poulose (2012). *Int. Nano Lett.* **2**, (1), 32.
54. P. Kanmani and J.-W. Rhim (2014). *Carbohydr. Polym.* **106**, 190–199.
55. B. Das, et al. (2017). *Arabian J. Chem.* **10**, (6), 862–876.
56. J. Saxena, et al. (2016). *SpringerPlus* **5**, (1), 1–10.
57. A. Muniyan, et al. (2017). *World J. Microbiol. Biotechnol.* **33**, (7), 147.
58. R. Thapa, et al. (2017). *Ann. Clin. Microbiol. Antimicrob.* **16**, (1), 39.
59. A. Banu and V. Rathod (2013). *Int. J. Biomed. Nanosci. Nanotechnol.* **3**, (1–2), 211–220.
60. M. Rai, et al. (2012). *J. Appl. Microbiol.* **112**, (5), 841–852.
61. S. Jana and T. Pal (2007). *J. Nanosci. Nanotechnol.* **7**, (6), 2151–2156.
62. H. Szmacinski, et al. (2008). *Appl. Spectrosc.* **62**, (7), 733–738.
63. R. Stiufiuc, et al. (2013). *Nanoscale Res. Lett.* **8**, (1), 47.
64. C. Malarkodi, et al. (2013). *Adv. Nano Res.* **1**, (2), 83–91.
65. A. Nalwade and A. Jadhav (2013). *Arch. Appl. Sci. Res.* **5**, (3), 45–49.
66. S. Ghosh, et al. (2012). *Int. J. Nanomed.* **7**, 483.
67. W. Schreurs and H. Rosenberg (1982). *J Bacteriol.* **152**, (1), 7–13.
68. C.-N. Lok, et al. (2006). *J. Proteome Res.* **5**, (4), 916–924.
69. S.-H. Kim, et al. (2011). Korean. *J. Microbiol. Biotechnol.* **39**, (1), 77–85.
70. J. Li, et al. (2013). *J. Nanosci. Nanotechnol.* **13**, (10), 6806–6813.
71. J. R. Morones, et al. (2005). *Nanotechnology* **16**, (10), 2346.
72. W. K. Jung, et al. (2008). *Appl. Environ. Microbiol.* **74**, (7), 2171–2178.
73. U. Klueh, et al. (2000). *J. Biomed. Mater. Res. A* **53**, (6), 621–631.
74. Y.-H. Hsueh et al. (2015). *PloS One* **10**(12).
75. D. Wu, et al. (2014). *J. Endod.* **40**, (2), 285–290.
76. C. Pellieux, et al. (2000). *Methods Enzymol.* **319**, 197–207.
77. P. K. Blecher and A. Friedman (2012). *J. Drugs Dermatol.* **11**, (7), 846–851.
78. S. Belluco et al. (2016). *Front. Microbiol.* **7**.
79. H. Xie, M. M. Mason, and J. P. Wise (2011). *Rev. Environ. Health* **26**, (4), 251–268.
80. J. Deutscher and M. H. Saier Jr. (2005). *J. Mol. Microbiol. Biotechnol.* **9**, (3–4), 125–131.
81. J. Kirstein and K. Turgay (2005). *J. Mol. Microbiol. Biotechnol.* **9**, (3–4), 182–188.
82. S. Shrivastava (2008). *Dig. J. Nanomater. Bios.* **3**, 303–308.
83. J. Tian, et al. (2007). *Chem. Med. Chem.* **2**, (1), 129–136.
84. Z.-M. Xiu, J. Ma, and P. J. Alvarez (2011). *Environ. Sci. Technol.* **45**, (20), 9003–9008.
85. A. L. Koch (1986). *J. Theor. Biol.* **120**, (1), 73–84.
86. G. Fujii, et al. (1997). *Biochemistry* **36**, (16), 4959–4968.
87. K.-J. Kim, et al. (2009). *Biometals* **22**, (2), 235–242.
88. F. J. Alvarez-Peral, et al. (2002). *Microbiology* **148**, (8), 2599–2606.